Chapter 9 Flow over Immersed Bodies

Fluid flows are broadly categorized:

1. Internal flows such as ducts/pipes, turbomachinery, open channel/river, which are bounded by walls or fluid interfaces: Chapter 8.

2. External flows such as flow around vehicles and structures, which are characterized by unbounded or partially bounded domains and flow field decomposition into viscous and inviscid regions: Chapter 9.

    a. Boundary layer flow: high Reynolds number flow around streamlines bodies without flow separation.

    $Re \le 1$: low Re flow (creeping or Stokes flow)
    $Re > \sim 1{,}000$: Laminar BL
    $Re > \sim 5\times10^5$ (Re_{crit}): Turbulent BL

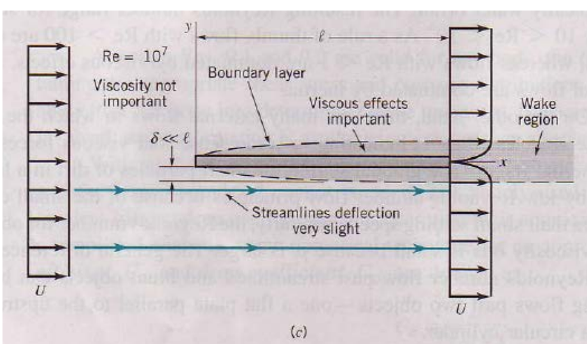

FIGURE 9.5 Character of the steady, viscous flow past a flat plate parallel to the upstream velocity: (*a*) low Reynolds number flow, (*b*) moderate Reynolds number flow, (*c*) large Reynolds number flow.

    b. Bluff body flow: flow around bluff bodies with flow separation.

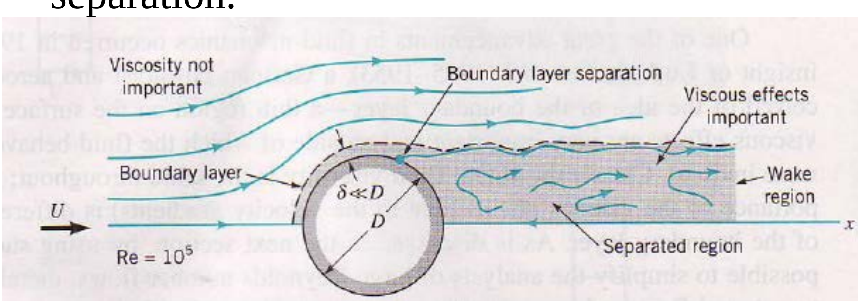

3. Free Shear flows such as jets, wakes, and mixing layers, which are also characterized by absence of walls and development and spreading in an unbounded or partially bounded ambient domain: advanced topic, which also uses boundary layer theory.

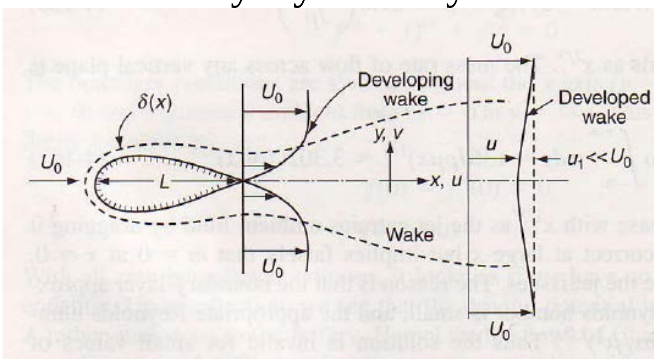

FIGURE 4-19
Flow in the wake of a body immersed in a stream.

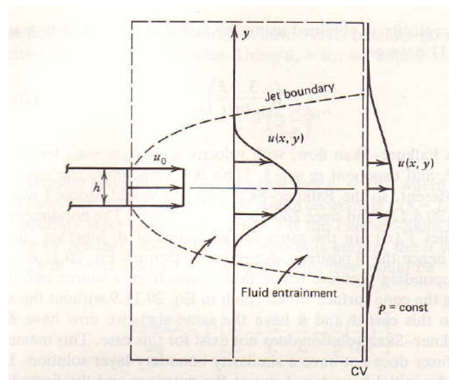

Figure 20.16 Plane laminar jet into an infinite medium.

Basic Considerations

Drag is decomposed into form and skin-friction contributions:

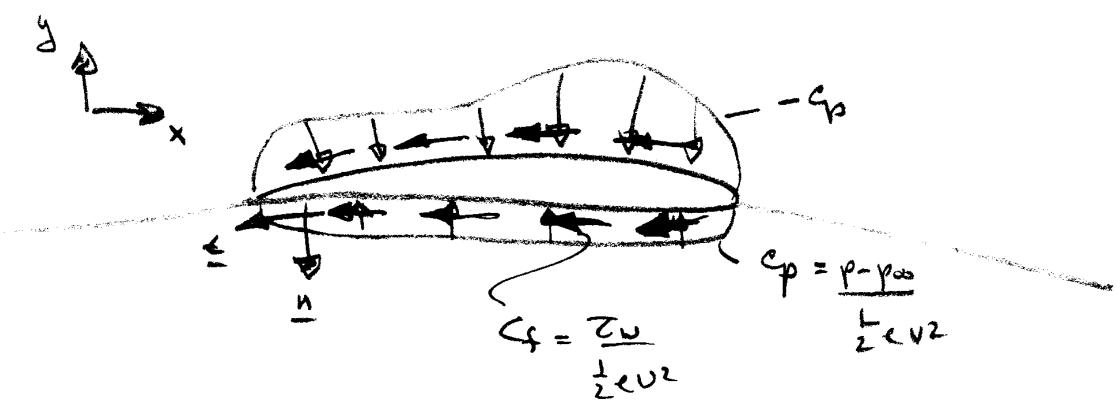

$$C_D = \frac{1}{\frac{1}{2}\rho V^2 A}\left\{\underbrace{\int_S (p-p_\infty)\underline{n}\cdot\hat{i}\,dA}_{C_{Dp}} + \underbrace{\int_S \tau_w \underline{t}\cdot\hat{i}\,dA}_{C_f}\right\}$$

$$C_L = \frac{1}{\frac{1}{2}\rho V^2 A}\left\{\int_S (p - p_\infty)\underline{n} \cdot \hat{j} dA\right\}$$

$\frac{t}{c} << 1 \quad C_f >> C_{Dp}$ streamlined body

$\frac{t}{c} \sim 1 \quad C_{Dp} >> C_f$ bluff body

Streamlining: One way to reduce the drag

→ reduce the flow separation→reduce the pressure drag
→ increase the surface area → increase the friction drag

→ Trade-off relationship between pressure drag and friction drag

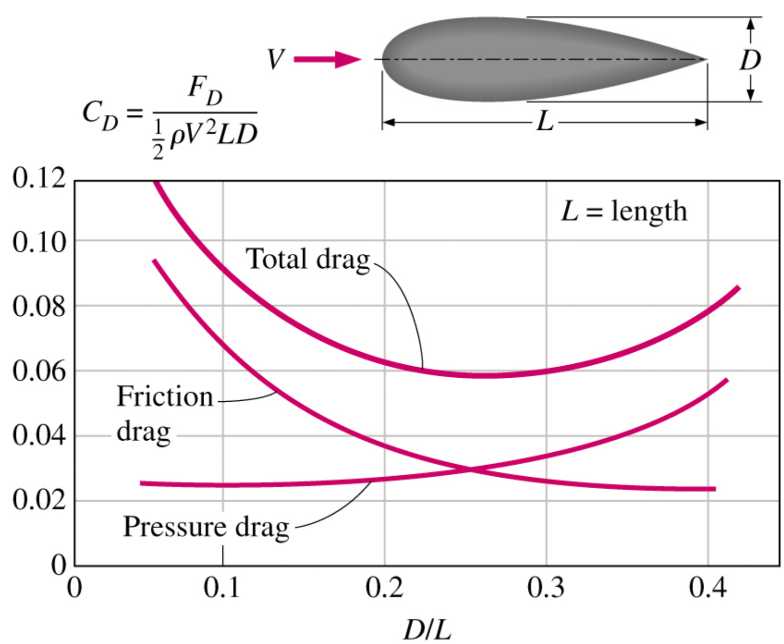

Trade-off relationship between pressure drag and friction drag

Benefit of streamlining: reducing vibration and noise

Qualitative Description of the Boundary Layer

Flow-field regions for high Re flow about slender bodies:

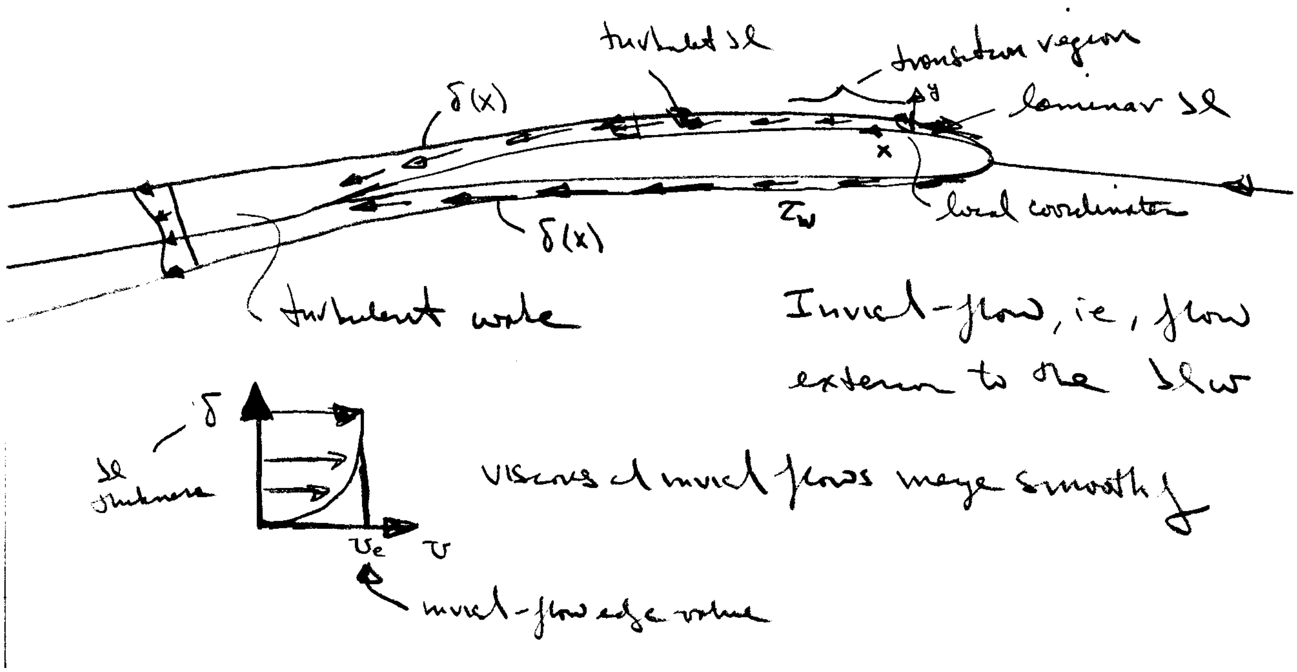

FIGURE 9.4
Development of boundary layer and distribution of shear stress along a thin, flat plate. (a) Flow pattern in boundary layers above and below the plate. (b) Shear-stress distribution on either side of the plate.

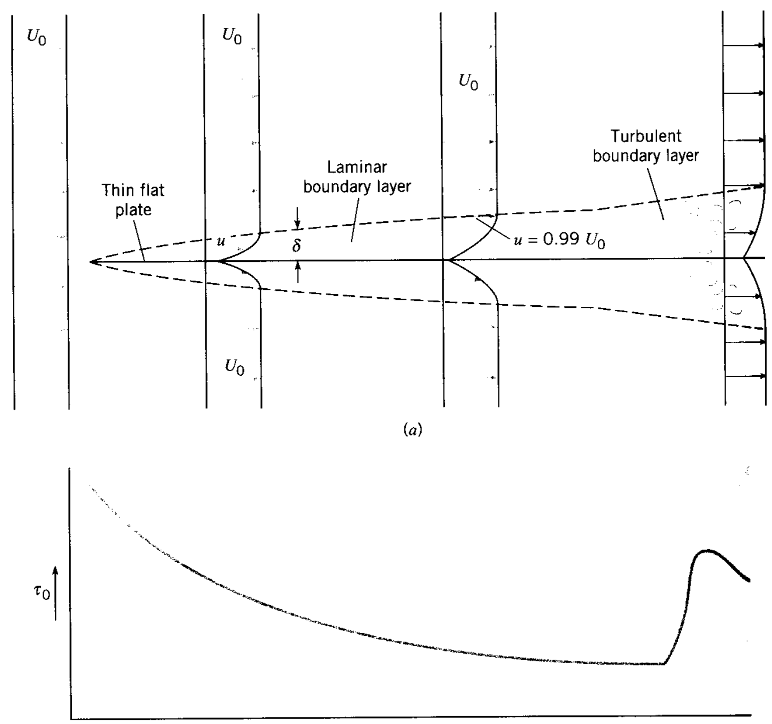

τ_w = shear stress

$\tau_w \propto$ rate of strain (velocity gradient)

$$= \mu \left.\frac{\partial u}{\partial y}\right|_{y=0}$$

large near the surface where fluid undergoes large changes to satisfy the no-slip condition

Boundary layer theory and equations are a simplified form of the complete NS equations and provides τ_w as well as a means of estimating C_{form}. Formally, boundary-layer theory represents the asymptotic form of the Navier-Stokes equations for high Re flow about slender bodies. The NS equations are 2^{nd} order nonlinear PDE and their solutions represent a formidable challenge. Thus, simplified forms have proven to be very useful.

Near the turn of the last century (1904), Prandtl put forth boundary-layer theory, which resolved D'Alembert's paradox: for inviscid flow drag is zero. The theory is restricted to unseparated flow. The boundary-layer equations are singular at separation, and thus, provide no information at or beyond separation. However, the requirements of the theory are met in many practical situations and the theory has many times over proven to be invaluable to modern engineering.

The assumptions of the theory are as follows:

Variable	order of magnitude		
u	U	$O(1)$	
v	$\delta<<L$	$O(\varepsilon)$	$\varepsilon = \delta/L$
$\frac{\partial}{\partial x}$	$1/L$	$O(1)$	
$\frac{\partial}{\partial y}$	$1/\delta$	$O(\varepsilon^{-1})$	
ν	δ^2	ε^2	

The theory assumes that viscous effects are confined to a thin layer close to the surface within which there is a dominant flow direction (x) such that $u \sim U$ and $v << u$. However, gradients across δ are very large in order to satisfy the no slip condition; thus, $\frac{\partial}{\partial y} >> \frac{\partial}{\partial x}$.

Next, we apply the above order of magnitude estimates to the NS equations.

$$\left.\begin{array}{l}
u\dfrac{\partial u}{\partial x}+v\dfrac{\partial u}{\partial y}=-\dfrac{\partial p}{\partial x}+\nu\left(\dfrac{\partial^2 u}{\partial x^2}+\dfrac{\partial^2 u}{\partial y^2}\right)\\
1\quad 1\qquad \varepsilon\quad \varepsilon^{-1}\qquad\qquad \varepsilon^{2}\quad 1\qquad \varepsilon^{-2}\\[2ex]
u\dfrac{\partial v}{\partial x}+v\dfrac{\partial v}{\partial y}=-\dfrac{\partial p}{\partial y}+\nu\left(\dfrac{\partial^2 v}{\partial x^2}+\dfrac{\partial^2 v}{\partial y^2}\right)\\
1\quad \varepsilon\qquad \varepsilon\quad 1\qquad\qquad \varepsilon^{2}\quad \varepsilon\qquad \varepsilon^{-1}\\[2ex]
\dfrac{\partial \mathrm{u}}{\partial \mathrm{x}}+\dfrac{\partial \mathrm{v}}{\partial \mathrm{y}}=0\\
1\qquad 1
\end{array}\right\}\ \text{elliptic}$$

Retaining terms of O(1) only results in the celebrated boundary-layer equations

$$\left.\begin{array}{l}
u\dfrac{\partial u}{\partial x}+v\dfrac{\partial u}{\partial y}=-\dfrac{\partial p}{\partial x}+\nu\dfrac{\partial^2 u}{\partial y^2}\\
\dfrac{\partial \mathrm{p}}{\partial \mathrm{y}}=0\\
\dfrac{\partial \mathrm{u}}{\partial \mathrm{x}}+\dfrac{\partial \mathrm{v}}{\partial \mathrm{y}}=0
\end{array}\right\}\ \text{parabolic}$$

Some important aspects of the boundary-layer equations:

1) the y-momentum equation reduces to

$$\frac{\partial p}{\partial y} = 0$$

i.e., $p = p_e =$ constant across the boundary layer

edge value, i.e., inviscid flow value!

from the Bernoulli equation:

$$p_e + \frac{1}{2}\rho U_e^2 = \text{constant}$$

i.e., $\dfrac{\partial p_e}{\partial x} = -\rho U_e \dfrac{\partial U_e}{\partial x}$

Thus, the boundary-layer equations are solved subject to a specified inviscid pressure distribution

2) continuity equation is unaffected

3) Although NS equations are fully elliptic, the boundary-layer equations are parabolic and can be solved using marching techniques

4) Boundary conditions

$u = v = 0 \qquad y = 0$

$u = U_e \qquad y = \delta$

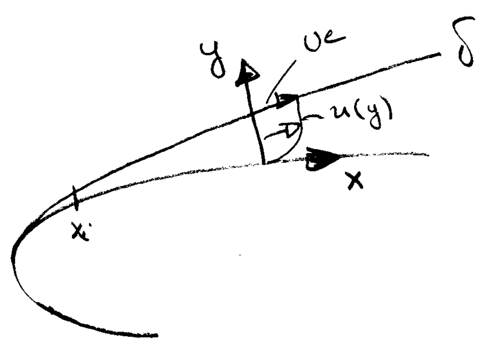

+ appropriate initial conditions @ x_i

There are quite a few analytic solutions to the boundary-layer equations. Also numerical techniques are available for arbitrary geometries, including both two- and three-dimensional flows. Here, as an example, we consider the simple, but extremely important case of the boundary layer development over a flat plate.

Quantitative Relations for the Laminar Boundary Layer

Laminar boundary-layer over a flat plate: Blasius solution (1908) student of Prandtl

$$\frac{\partial u}{\partial x}+\frac{\partial v}{\partial y}=0$$

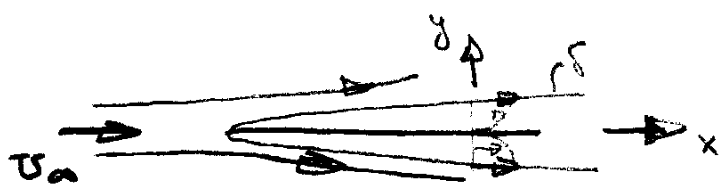

Note: $\frac{\partial p}{\partial x}=0$ for a flat plate

$$u\frac{\partial u}{\partial x}+v\frac{\partial u}{\partial y}=\nu\frac{\partial^2 u}{\partial y^2}$$

$$u = v = 0 \ @\ y = 0 \qquad u = U_\infty \ @\ y = \delta$$

We now introduce a dimensionless transverse coordinate and a stream function, i.e.,

$$\eta = y\sqrt{\frac{U_\infty}{\nu x}} \propto \frac{y}{\delta}$$

$$\psi = \sqrt{\nu x U_\infty}\, f(\eta)$$

$$u = \frac{\partial \psi}{\partial y} = \frac{\partial \psi}{\partial \eta}\frac{\partial \eta}{\partial y} = U_\infty f'(\eta) \qquad\qquad f' = u/U_\infty$$

$$v = -\frac{\partial \psi}{\partial x} = \frac{1}{2}\sqrt{\frac{\nu U_\infty}{x}}\left(\eta f' - f\right)$$

Substitution into the boundary-layer equations yields

$$ff'' + 2f''' = 0 \qquad\qquad \text{Blasius Equation}$$
$$f = f' = 0 \quad @\ \eta = 0 \qquad\qquad f' = 1 \quad @\ \eta \to \infty$$

The Blasius equation is a 3rd order ODE which can be solved by standard methods (Runge-Kutta). Also, series solutions are possible. Interestingly, although simple in appearance no analytic solution has yet been found. Finally, it should be recognized that the Blasius solution is a similarity solution, i.e., the non-dimensional velocity profile f' vs. η is independent of x. That is, by suitably scaling all the velocity profiles have neatly collapsed onto a single curve.

Now, lets consider the characteristics of the Blasius solution:

$$\frac{u}{U_\infty} \text{ vs. } y$$

$$\frac{v}{U_\infty} \text{ vs. } y$$

$$\delta = \frac{5x}{\sqrt{\text{Re}_x}}$$ value of y where $u/U_\infty = .99$

$$\text{Re}_x = \frac{U_\infty x}{\nu}$$

FIGURE 9.5
Velocity distribution in laminar boundary layer. [After Blasius (3)].

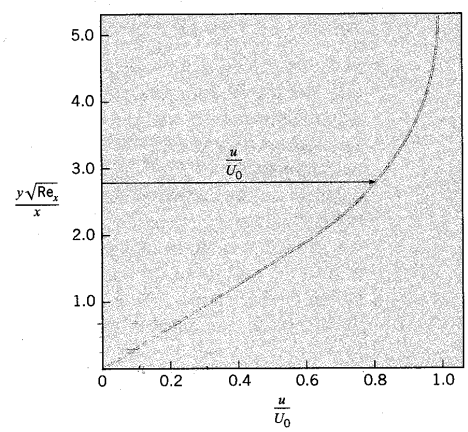

TABLE 9.1 RESULTS—δ AND τ_0 FOR DIFFERENT VALUES OF x

	x = 0.1 ft	x = 1.0 ft	x = 2 ft	x = 4 ft	x = 6 ft
$x^{1/2}$	0.316	1.00	1.414	2.00	2.45
τ_0, psf	0.552	0.174	0.123	0.087	0.071
δ, ft	0.005	0.016	0.022	0.031	0.039
δ, in.	0.060	0.189	0.270	0.380	0.466

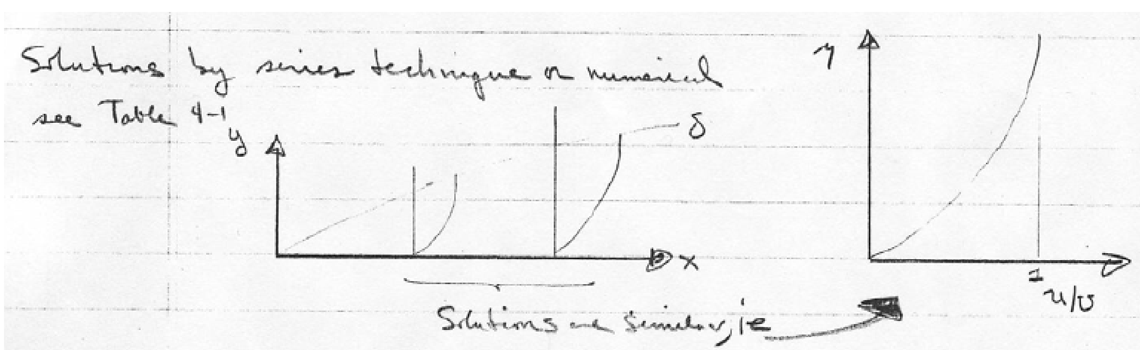

$$\tau_w = \frac{\mu U_\infty f''(0)}{\sqrt{2\nu x / U_\infty}}$$

see below

i.e., $$c_f = \frac{2\tau_w}{\rho U_\infty^2} = \frac{0.664}{\sqrt{\mathrm{Re}_x}} = \frac{\theta}{x}$$: Local friction coeff.

$$C_f = \frac{b}{bL}\int_0^L c_f\, dx = 2c_f(L)$$: Friction drag coeff.

$$= \frac{1.328}{\sqrt{\mathrm{Re}_L}} \qquad \frac{U_\infty L}{\nu}$$

Note:
b = plate width
L = plate length

Wall shear stress: $\tau_w = 0.332 U_\infty^{3/2}\sqrt{\frac{\rho\mu}{x}}$ or $\tau_w = 0.332\mu\left(U_\infty / x\right)\sqrt{\mathrm{Re}_x}$

Other:

$$\delta^* = \int_0^\delta \left(1 - \frac{u}{U_\infty}\right) dy = 1.7208\frac{x}{\sqrt{\mathrm{Re}_x}}$$ displacement thickness

measure of displacement of inviscid flow due to boundary layer

$$\theta = \int_0^\delta \left(1 - \frac{u}{U_\infty}\right)\frac{u}{U_\infty} dy = 0.664\frac{x}{\sqrt{\mathrm{Re}_x}}$$ momentum thickness

measure of loss of momentum due to boundary layer

H = shape parameter = $\frac{\delta^*}{\theta}$=2.5916

TABLE 4-1
Numerical solution of the Blasius flat-plate relation, Eq. (4-45)

η	$f(\eta)$	$f'(\eta)$	$f''(\eta)$
0.0	0.0	0.0	0.46960
0.1	0.00235	0.04696	0.46956
0.2	0.00939	0.09391	0.46931
0.3	0.02113	0.14081	0.46861
0.4	0.03755	0.18761	0.46725
0.5	0.05864	0.23423	0.46503
0.6	0.08439	0.28058	0.46173
0.7	0.11474	0.32653	0.45718
0.8	0.14967	0.37196	0.45119
0.9	0.18911	0.41672	0.44363
1.0	0.23299	0.46063	0.43438
1.1	0.28121	0.50354	0.42337
1.2	0.33366	0.54525	0.41057
1.3	0.39021	0.58559	0.39598
1.4	0.45072	0.62439	0.37969
1.5	0.51503	0.66147	0.36180
1.6	0.58296	0.69670	0.34249
1.7	0.65430	0.72993	0.32195
1.8	0.72887	0.76106	0.30045
1.9	0.80644	0.79000	0.27825
2.0	0.88680	0.81669	0.25567
2.2	1.05495	0.86330	0.21058
2.4	1.23153	0.90107	0.16756
2.6	1.41482	0.93060	0.12861
2.8	1.60328	0.95288	0.09511
3.0	1.79557	0.96905	0.06771
3.2	1.99058	0.98037	0.04637
3.4	2.18747	0.98797	0.03054
3.6	2.38559	0.99289	0.01933
3.8	2.58450	0.99594	0.01176
4.0	2.78388	0.99777	0.00687
4.2	2.98355	0.99882	0.00386
4.4	3.18338	0.99940	0.00208
4.6	3.38329	0.99970	0.00108
4.8	3.58325	0.99986	0.00054

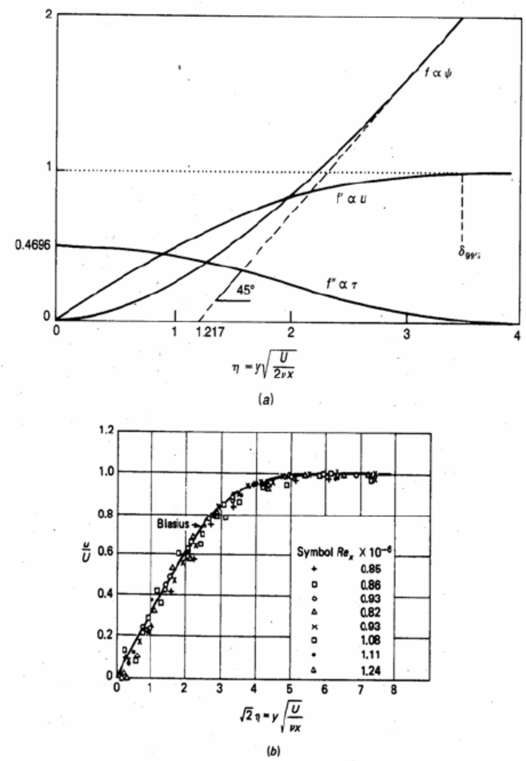

FIGURE 4-6
The Blasius solution for the flat-plate boundary layer: (*a*) numerical solution of Eq. (4-45); (*b*) comparison of $f' = u/U$ with experiments by Liepmann (1943).

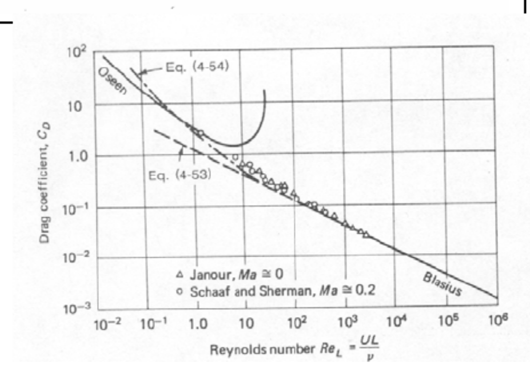

Quantitative Relations for the Turbulent Boundary Layer

2-D Boundary-layer Form of RANS equations

$$\frac{\partial u}{\partial x}+\frac{\partial v}{\partial y}=0$$

$$u\frac{\partial u}{\partial x}+v\frac{\partial u}{\partial y}=-\frac{\partial}{\partial x}\left(\frac{p_e}{\rho}\right)+\nu\frac{\partial^2 u}{\partial y^2}-\underbrace{\frac{\partial}{\partial y}\left(\overline{u'v'}\right)}_{\text{requires modeling}}$$

Momentum Integral Analysis

Historically similarity and AFD methods used for idealized flows and momentum integral methods for practical applications, including pressure gradients. Modern approach: CFD.

To obtain general momentum integral relation which is valid for both laminar and turbulent flow

$$\int_{y=0}^{\infty}\left(\text{momentum equation}+(u-v)\,\text{continuity}\right)dy$$

For flat plate or δ for general case

$$\underbrace{\frac{\tau_w}{\rho U^2}=\frac{1}{2}c_f=\frac{d\theta}{dx}}_{\text{flat plate equation }\frac{dU}{dx}=0}+(2+H)\frac{\theta}{U}\frac{dU}{dx} \qquad -\frac{dp}{dx}=\rho U\frac{dU}{dx}$$

$$\theta = \int_0^\delta \frac{u}{U}\left(1-\frac{u}{U}\right)dy$$ momentum thickness

$$H = \frac{\delta^*}{\theta}$$ shape parameter

$$\delta^* = \int_0^\delta \left(1-\frac{u}{U}\right)dy$$ displacement thickness

Can also be derived by CV analysis as shown next for flat plate boundary layer.

Momentum Equation Applied to the Boundary Layer

Consider flow of a viscous fluid at high Re past a flat plate, i.e., flat plate fixed in a uniform stream of velocity $U\hat{i}$.

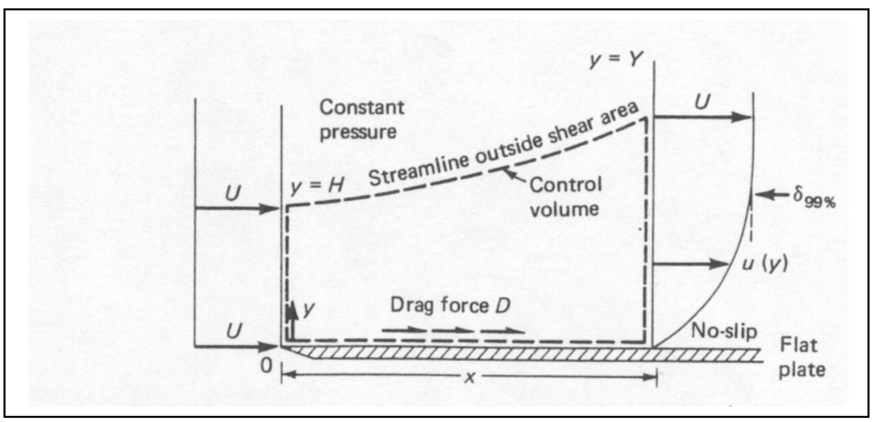

Boundary-layer thickness arbitrarily defined by y = $\delta_{99\%}$ (where, $\delta_{99\%}$ is the value of y at u = 0.99U). Streamlines outside $\delta_{99\%}$ will deflect an amount δ^* (**the displacement thickness**). Thus the streamlines move outward from $y = H$ at $x = 0$ to $y = Y = \delta = H + \delta^*$ at $x = x_1$.

Conservation of mass:

$$\int_{CS} \rho \underline{V} \bullet \underline{n} dA = \mathbf{0} = -\int_0^H \rho U dy + \int_0^{H+\delta^*} \rho u dy$$

Assume incompressible flow (constant density):

$$UH = \int_0^Y u dy = \int_0^Y (U + u - U) dy = UY + \int_0^Y (u - U) dy$$

Substituting $Y = H + \delta^*$ defines displacement thickness:

$$\delta^* = \int_0^Y \left(1 - \frac{u}{U}\right) dy$$

δ^* is an important measure of effect of BL on external flow.
Consider alternate derivation based on equivalent flow rate:

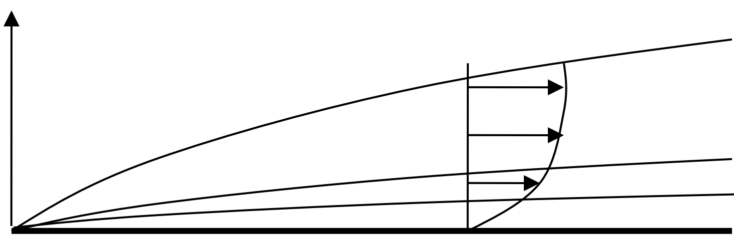

$$\underbrace{\int_{\delta^*}^{\delta} U dy}_{\text{Inviscid flow about } \delta^* \text{ body}} = \int_0^{\delta} u dy$$

Flowrate between δ^* and δ of inviscid flow=actual flowrate, i.e., inviscid flow rate about displacement body = viscous flow rate about actual body

$$\int_0^{\delta} U dy - \int_0^{\delta^*} U dy = \int_0^{\delta} u dy \Rightarrow \delta^* = \int_0^{\delta} \left(1 - \frac{u}{U}\right) dy$$

w/o BL - displacement effect=actual discharge

For 3D flow, in addition it must also be explicitly required that δ^* is a stream surface of the inviscid flow continued from outside of the BL.

<u>Conservation of x-momentum</u>:

$$\sum F_x = -D = \int_{CS} \rho u \underline{V} \bullet \underline{n} dA = -\int_0^H \rho U(Udy) + \int_0^Y \rho u(udy)$$

$$Drag = D = \rho U^2 H - \int_0^Y \rho u^2 dy$$

= Fluid force on plate = - Plate force on CV (fluid)

Again assuming constant density and using continuity:

$$H = \int_0^Y \frac{u}{U} dy$$

$$D = \rho U^2 \int_0^Y u/U dy - \rho \int_0^Y u^2 dy = \int_0^x \tau_w dx$$

$$\frac{D}{\rho U^2} = \theta = \int_0^Y \frac{u}{U}\left(1 - \frac{u}{U}\right) dy$$

where, θ is the **momentum thickness (a function of x only)**, an important measure of the drag.

$$C_D = \frac{2D}{\rho U^2 x} = \frac{2\theta}{x} = \frac{1}{x}\int_0^x c_f dx$$ Per unit span

$$c_f = \frac{\tau_w}{\frac{1}{2}\rho U^2} \Rightarrow c_f = \frac{d}{dx}(xC_D) = 2\frac{d\theta}{dx}$$

$$\frac{d\theta}{dx} = \frac{c_f}{2} \qquad \tau_w = \rho U^2 \frac{d\theta}{dx}$$

Special case 2D momentum integral equation for dp/dx = 0

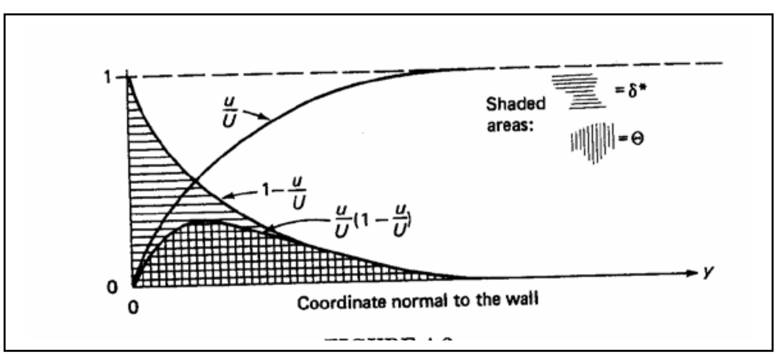

Simple velocity profile approximations:

$$u = U(2y/\delta - y^2/\delta^2)$$

$u(0) = 0$ no slip

$\left.\begin{array}{l} u(\delta) = U \\ u_y(\delta)=0 \end{array}\right\}$ matching with outer flow

Use velocity profile to get $C_f(\delta)$ and $\theta(\delta)$ and then integrate momentum integral equation to get $\delta(Re_x)$

$\delta^* = \delta/3$
$\theta = 2\delta/15$
$H= \delta^*/\theta= 5/2$

$$\tau_w = 2\mu U/\delta$$

$$\Rightarrow c_f = \frac{2\mu U/\delta}{1/2\rho U^2} = 2\frac{d\theta}{dx} = 2\frac{d}{dx}(2\delta/15)$$

$$\therefore \delta d\delta = \frac{15\mu dx}{\rho U}$$

$$\delta^2 = \frac{30\mu dx}{\rho U}$$

$$\left.\begin{array}{l} \delta/x = 5.5/\mathrm{Re}_x^{1/2} \\ \mathrm{Re}_x = Ux/\nu; \\ \delta^*/x = 1.83/\mathrm{Re}_x^{1/2} \\ \theta/x = 0.73/\mathrm{Re}_x^{1/2} \\ C_D = 1.46/\mathrm{Re}_L^{1/2} = 2C_f(L) \end{array}\right\} \text{10\% error, cf. Blasius}$$

Approximate solution Turbulent Boundary-Layer

$Re_t = 5\times10^5 \sim 3\times10^6$ for a flat plate boundary layer

$Re_{crit} \sim 100{,}000$

$$\frac{c_f}{2} = \frac{d\theta}{dx}$$

as was done for the approximate laminar flat plate boundary-layer analysis, solve by expressing $c_f = c_f(\delta)$ and $\theta = \theta(\delta)$ and integrate, i.e. assume log-law valid across entire turbulent boundary-layer

$$\frac{u}{u^*} = \frac{1}{\kappa}\ln\frac{yu^*}{\nu} + B$$

neglect laminar sub layer and velocity defect region

at $y = \delta$, $u = U$

$$\frac{U}{u^*} = \frac{1}{\kappa}\ln\underbrace{\frac{\delta u^*}{\nu}}_{Re_\delta\left(\frac{c_f}{2}\right)^{1/2}} + B$$

or $$\left(\frac{2}{c_f}\right)^{1/2} = 2.44\ln\left[Re_\delta\left(\frac{c_f}{2}\right)^{1/2}\right] + 5$$

$$c_f \cong .02\,Re_\delta^{-1/6} \quad \text{power-law fit}$$

$c_f(\delta)$

Next, evaluate

$$\frac{d\theta}{dx} = \frac{d}{dx}\int_0^\delta \frac{u}{U}\left(1-\frac{u}{U}\right)dy$$

can use log-law or more simply a power law fit

$$\left.\begin{aligned} &\frac{u}{U} = \left(\frac{y}{\delta}\right)^{1/7} \\ &\theta = \frac{7}{72}\delta = \theta(\delta) \end{aligned}\right\}$$

Note: cannot be used to obtain $c_f(\delta)$ since $\tau_w \to \infty$

$$\Rightarrow \qquad \tau_w = c_f \frac{1}{2}\rho U^2 = \rho U^2 \frac{d\theta}{dx} = \frac{7}{72}\rho U^2 \frac{d\delta}{dx}$$

$$Re_\delta^{-1/6} = 9.72\frac{d\delta}{dx}$$

or $\quad \dfrac{\delta}{x} = 0.16\,Re_x^{-1/7}$

$\delta \propto x^{6/7}$ almost linear

i.e., much faster growth rate than laminar boundary layer

$$c_f = \frac{0.027}{Re_x^{1/7}}$$

$$C_f = \frac{0.031}{Re_L^{1/7}} = \frac{7}{6}c_f(L)$$

These formulas are for a fully turbulent flow over a smooth flat plate from the leading edge; in general, give better results for sufficiently large Reynolds number $Re_L > 10^7$.

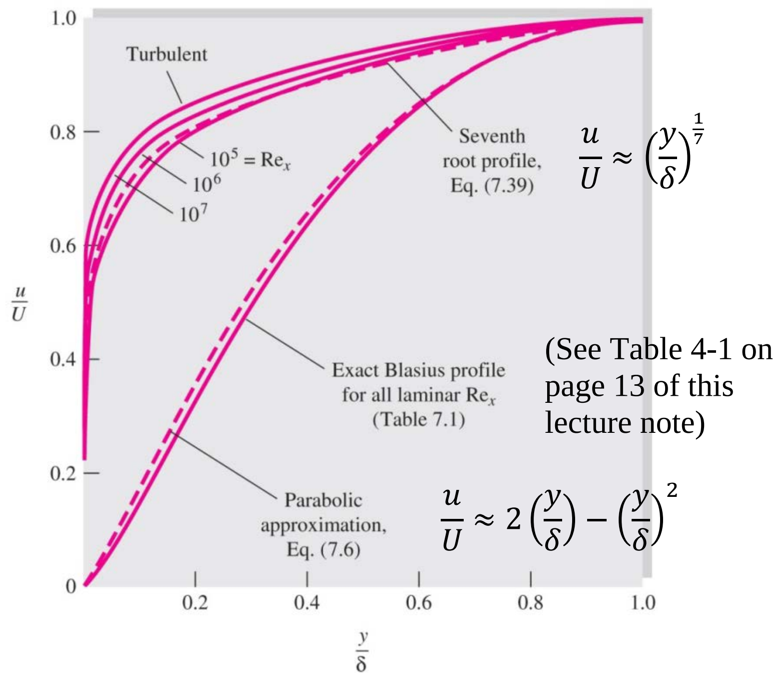

Comparison of dimensionless laminar and turbulent flat-plate velocity profiles (Ref: White, F. M., Fluid Mechanics, 7th Ed., McGraw-Hill)

Alternate forms by using the same velocity profile $u/U = (y/\delta)^{1/7}$ assumption but using an experimentally determined shear stress formula $\tau_w = 0.0225\rho U^2(\nu/U\delta)^{1/4}$ are:

$$\frac{\delta}{x} = 0.37\,\mathrm{Re}_x^{-1/5} \qquad c_f = \frac{0.058}{\mathrm{Re}_x^{1/5}} \qquad C_f = \frac{0.074}{\mathrm{Re}_L^{1/5}}$$

shear stress: $$\tau_w = \frac{0.029\rho U^2}{\mathrm{Re}_x^{1/5}}$$

These formulas are valid only in the range of the experimental data, which covers $\mathrm{Re}_L = 5 \times 10^5 \sim 10^7$ for smooth flat plates.

Other empirical formulas are by using the logarithmic velocity-profile instead of the 1/7-power law:

$$\frac{\delta}{L} = c_f(0.98 \log Re_L - 0.732)$$

$$c_f = (2 \log Re_x - 0.65)^{-2.3}$$

$$C_f = \frac{0.455}{(\log_{10} Re_L)^{2.58}}$$

These formulas are also called as the *Prandtl-Schlichting skin-friction formula* and valid in the whole range of $Re_L \leq 10^9$.

For these experimental/empirical formulas, the boundary layer is usually "tripped" by some roughness or leading edge disturbance, to make the boundary layer turbulent from the leading edge.

No definitive values for turbulent conditions since depend on empirical data and turbulence modeling.

Finally, composite formulas that take into account both the initial laminar boundary layer and subsequent turbulent boundary layer, i.e. in the transition region ($5 \times 10^5 < Re_L < 8 \times 10^7$) where the laminar drag at the leading edge is an appreciable fraction of the total drag:

$$C_f = \frac{0.031}{Re_L^{\frac{1}{7}}} - \frac{1440}{Re_L}$$

$$C_f = \frac{0.074}{Re_L^{\frac{1}{5}}} - \frac{1700}{Re_L}$$

$$C_f = \frac{0.455}{(\log_{10} Re_L)^{2.58}} - \frac{1700}{Re_L}$$

with transitions at $Re_t = 5 \times 10^5$ for all cases.

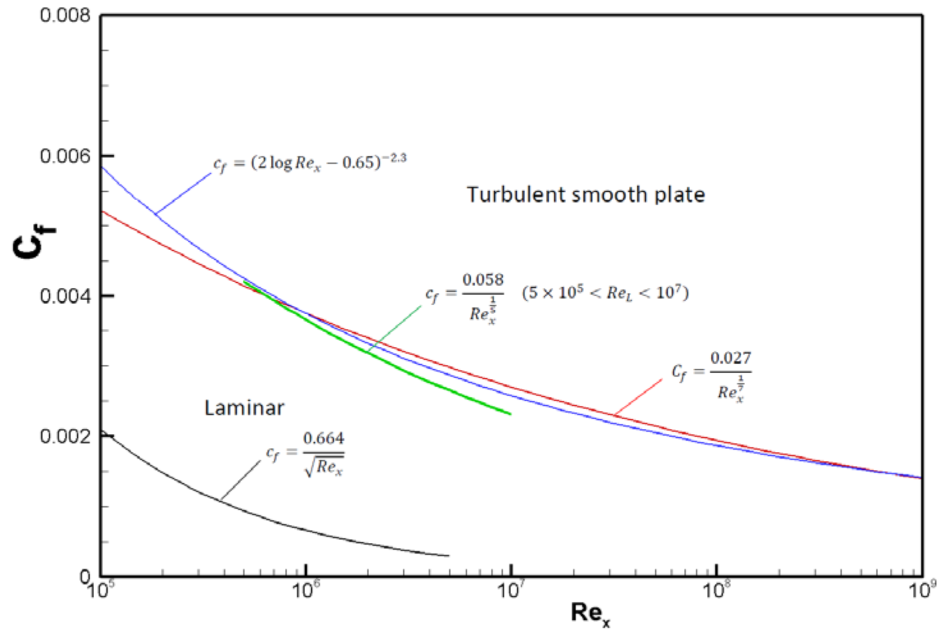

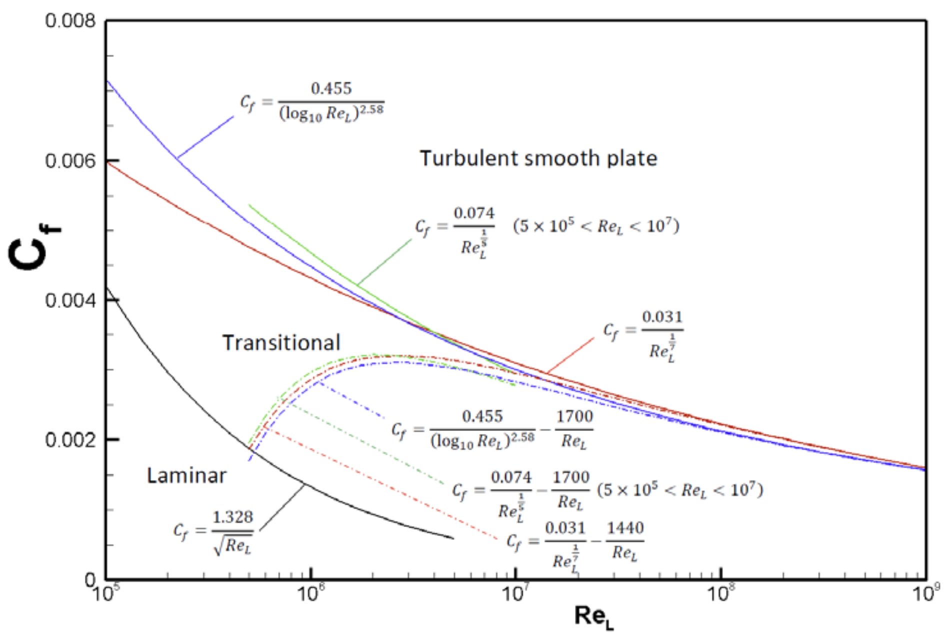

Local friction coefficient c_f (top) and friction drag coefficient C_f (bottom) for a flat plate parallel to the upstream flow.

Bluff Body Drag

Drag of 2-D Bodies

First consider a flat plate both parallel and normal to the flow

$$C_{Dp} = \frac{1}{\frac{1}{2}\rho V^2 A}\int_S (p - p_\infty)\underline{n}\cdot\hat{i} = 0$$

$$C_f = \frac{1}{\frac{1}{2}\rho V^2 A}\int_S \tau_w \underline{t}\cdot\hat{i}dA$$

$$= \frac{1.33}{Re_L^{1/2}} \qquad \text{laminar flow}$$

$$= \frac{.074}{Re_L^{1/5}} \qquad \text{turbulent flow}$$

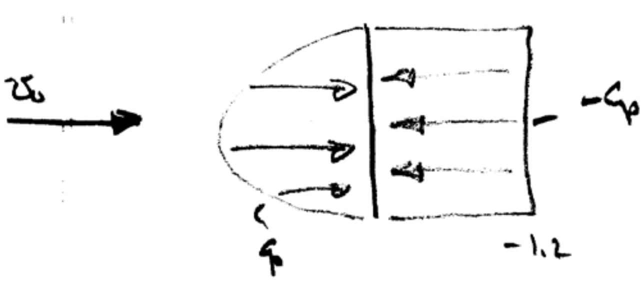

flow pattern

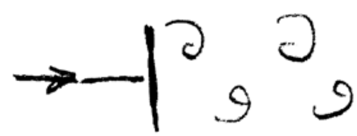

vortex wake
typical of bluff body flow

where C_p based on experimental data

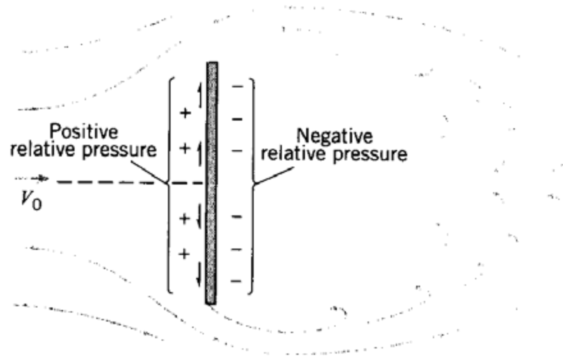

FIGURE 11.3
Flow past a flat plate.

FIGURE 11.4
Pressure distribution on a plate normal to the approach flow for $Re > 10^4$.

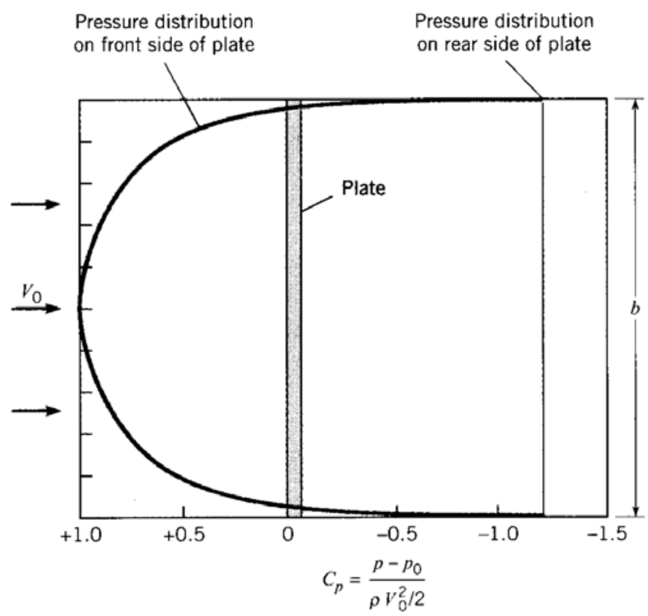

$$C_{Dp} = \frac{1}{\frac{1}{2}\rho V^2 A} \int_S (p - p_\infty)\underline{n} \cdot \hat{i} dA$$

$$= \frac{1}{A}\int_S C_p dA$$

$= 2$ using numerical integration of experimental data

$C_f = 0$

For bluff body flow experimental data used for C_D.

In general, Drag = f(V, L, ρ, μ, c, t, ε, T, etc.)
from dimensional analysis

$$\underbrace{C_D = \frac{\text{Drag}}{\frac{1}{2}\rho V^2 A}}_{\text{scale factor}} = f\left(\text{Re}, \overset{c/L}{\text{Ar}}, \frac{t}{L}, \frac{\varepsilon}{L}, \text{T, etc.}\right)$$

DRAG ON IMMERSED BODIES

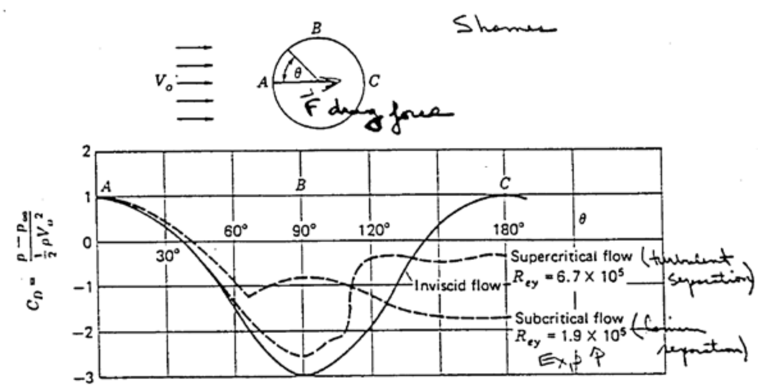

Figure 10.23 Pressure distributions around a cylinder for subcritical, supercritical, and inviscid flows.

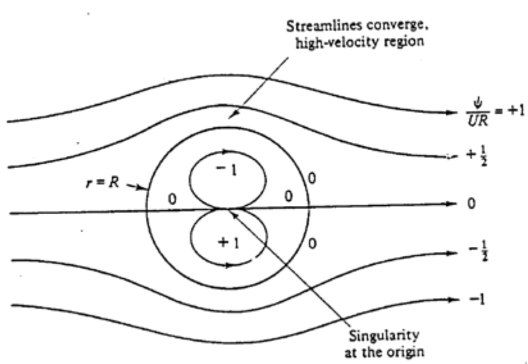

Fig. E4.7

Potential Flow Solution: $\psi = -U_\infty\left(r - \frac{a^2}{r}\right)\sin\theta$

$$p + \frac{1}{2}\rho V^2 = p_\infty + \frac{1}{2}\rho U_\infty^2 \qquad u_r = \frac{1}{r}\frac{\partial\psi}{\partial\theta}$$

$$C_p = \frac{p - p_\infty}{\frac{1}{2}\rho U_\infty^2} = 1 - \frac{u_r^2 + u_\theta^2}{U_\infty^2} \qquad u_\theta = -\frac{\partial\psi}{\partial r}$$

$$C_p(r = a) = 1 - 4\sin^2\theta \longleftarrow \text{surface pressure}$$

Flow Separation

Flow separation:

→The fluid stream detaches itself from the surface of the body at sufficiently high velocities. Only appeared in viscous flow!!

Flow separation forms the region called 'separated region'

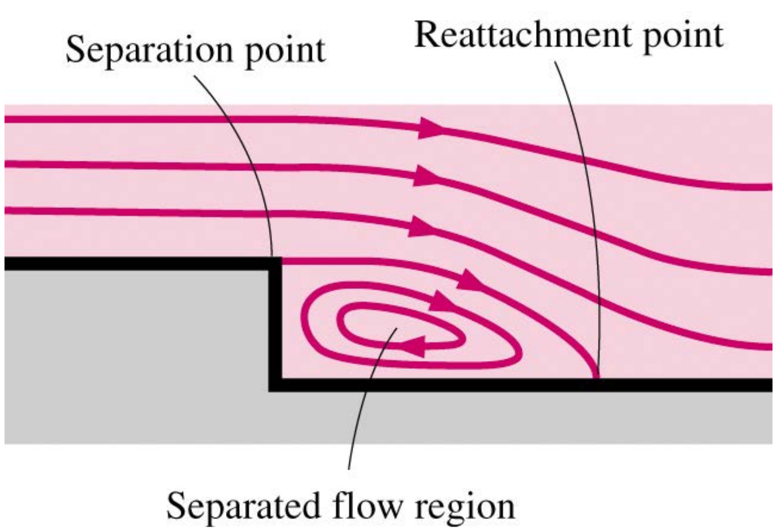

Inside the separation region:
→low-pressure, existence of recirculating/backflows
→viscous and rotational effects are the most significant!

Important physics related to flow separation:
→'Stall' for airplane (Recall the movie you saw at CFD-PreLab2!)
→Vortex shedding
(Recall your work at CFD-Lab2, AOA=16°! What did you see in your velocity-vector plot at the trailing edge of the air foil?)

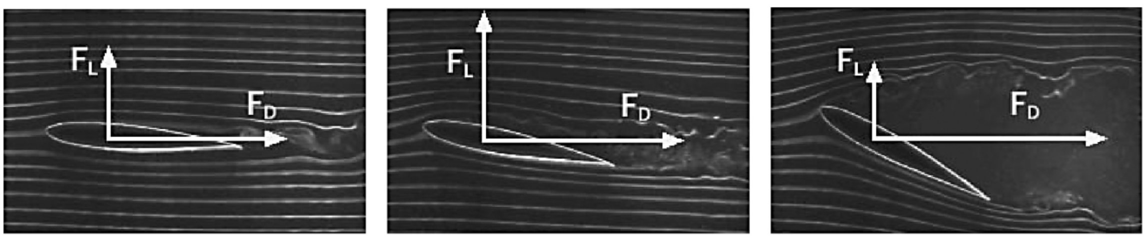

(*a*) 5° (*b*) 15° (*c*) 30°

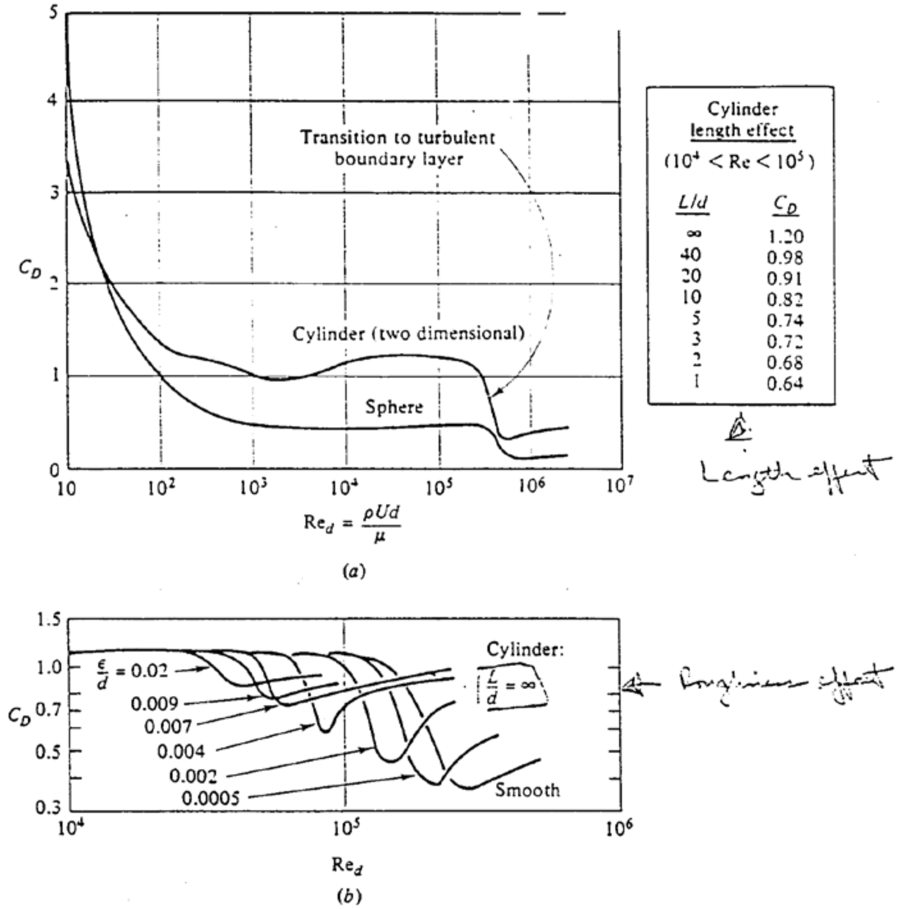

Fig. 5.3 The proof of practical dimensional analysis: drag coefficients of a cylinder and sphere: (*a*) drag coefficient of a smooth cylinder and sphere (data from many sources); (*b*) increased roughness causes earlier transition to a turbulent boundary layer.

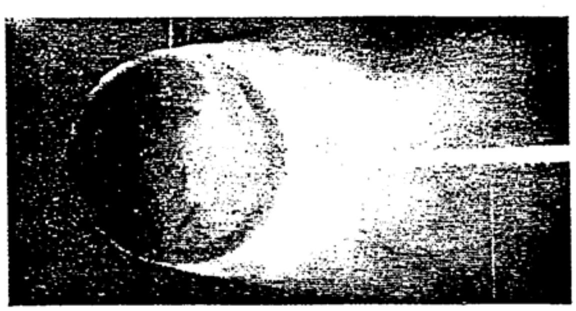

FIG. 34.—Flow round sphere below critical point. (*Wieselsberger.*)

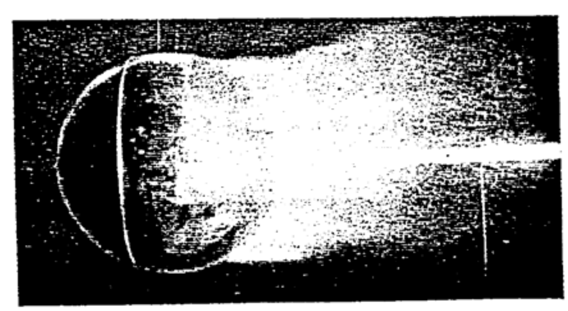

FIG. 35.—Owing to a thin wire ring round the sphere, the flow becomes of the other type with turbulent boundary layer. (*Wieselsberger.*)

426 XV. Non-steady boundary layers

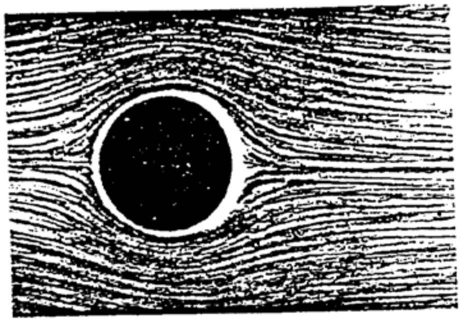

Fig. 15.5a

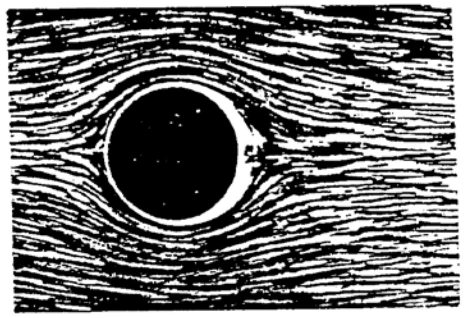

Fig. 15.5b

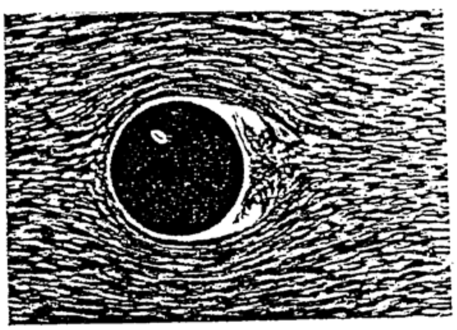

Fig. 15.5c

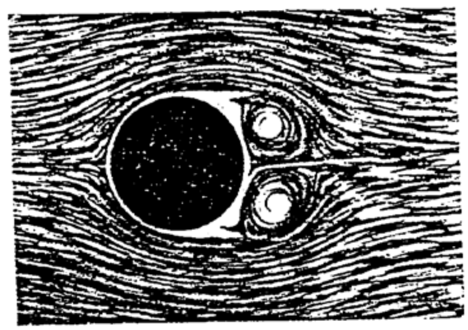

Fig. 15.5d

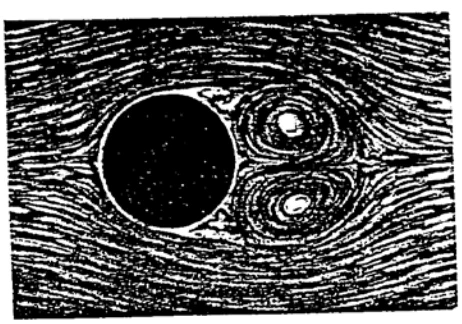

Fig. 15.5e

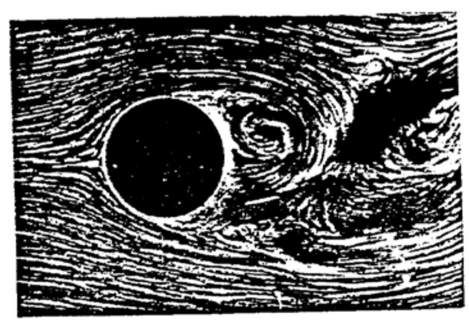

Fig. 15.5f

Fig. 15.5 a to f. Formation of vortices in flow past a circular cylinder after acceleration from rest (L. Prandtl)

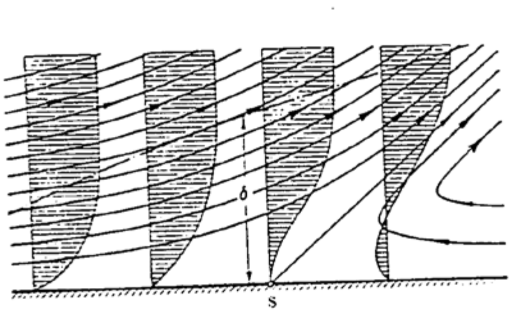

S = point of separation

Fig. 2.12. Diagrammatic representation of flow in the boundary layer near a point of separation

alternate formation and shedding of vortices also creates a regular change in pressure with consequent periodicity in side thrust on the cylinder. Vortex shedding was the primary cause of failure of the Tacoma Narrows suspension bridge in the state of Washington in 1940. Another, more commonplace, effect of vortex shedding is the "singing" of wires in the wind.

If the frequency of the vortex shedding is in resonance with the natural frequency of the member that produces it, large amplitudes of vibration with consequent large stresses can develop. Experiments show that the frequency of shedding is given in terms of the Strouhal number S, and this in turn is a function of the Reynolds number. Here the Strouhal number is defined as

$$S = \frac{nd}{V_0} \tag{11-7}$$

where n is the frequency of shedding of vortices from one side of cylinder, in Hz, d is the diameter of cylinder, and V_0 is the free-stream velocity.

The relationship between the Strouhal number and the Reynolds number for vortex shedding from a circular cylinder is given in Fig. 11-10.

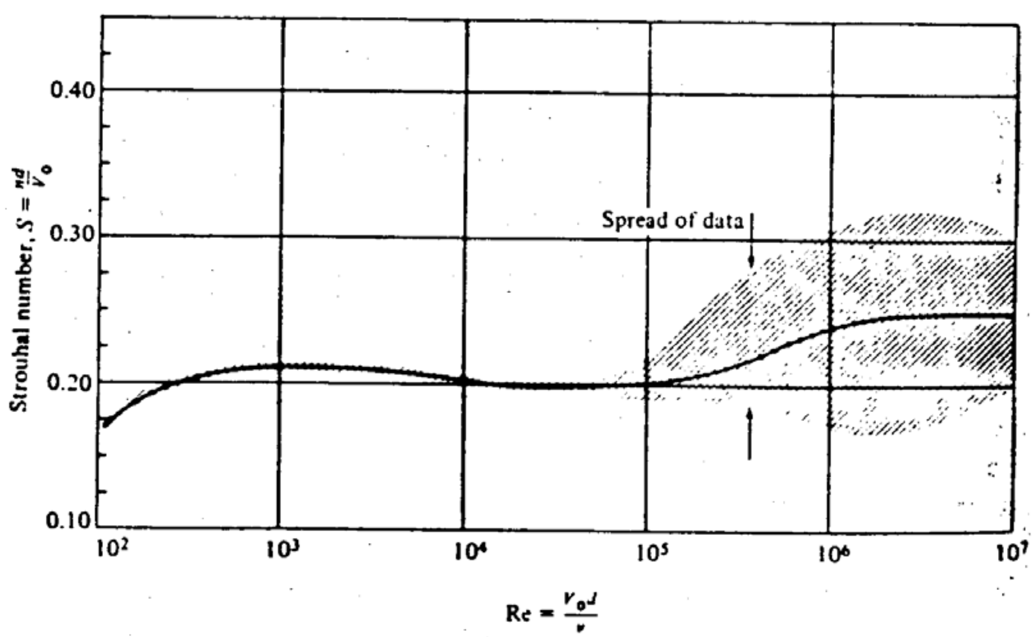

FIGURE 11-10 Strouhal number versus Reynolds number for flow past a circular cylinder. [After Jones (14) and Roshko (23)]

Other cylindrical and two-dimensional bodies also shed vortices. Consequently, the engineer should always be alert to vibration problems when designing structures that are exposed to wind or water flow.

EXAMPLE 11-2 For the cylinder and conditions of Example 11-1, at what frequency will the vortices be shed?

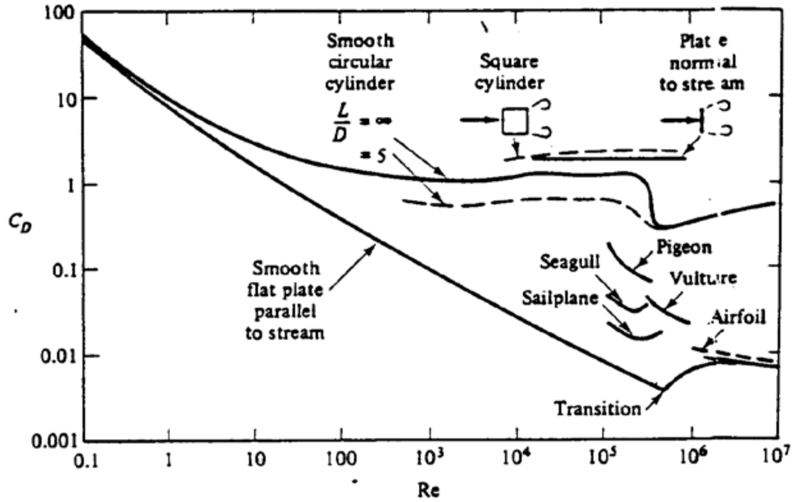

Fig. 7.16 Drag versus Reynolds number for nearly two-dimensional bodies.

Table 7.2
DRAG OF TWO-DIMENSIONAL BODIES AT Re = 10^5

Shape	*C_D based on frontal area*	*Shape*	*C_D based on frontal area*
Plate: (flow → flat plate)	2.0	Half-cylinder: (flow → flat side)	1.2
Square cylinder: (flow → face)	2.1	(flow → round side)	1.7
(flow → corner)	1.6	Equilateral triangle: (flow → flat side)	1.6
Half tube: (flow → open side)	1.2	(flow → apex)	2.0
(flow → convex side)	2.3		

Elliptical cylinder:	*Laminar*	*Turbulent*
1:1	1.2	0.3
2:1	0.6	0.2
4:1	0.35	0.15
8:1	0.25	0.1

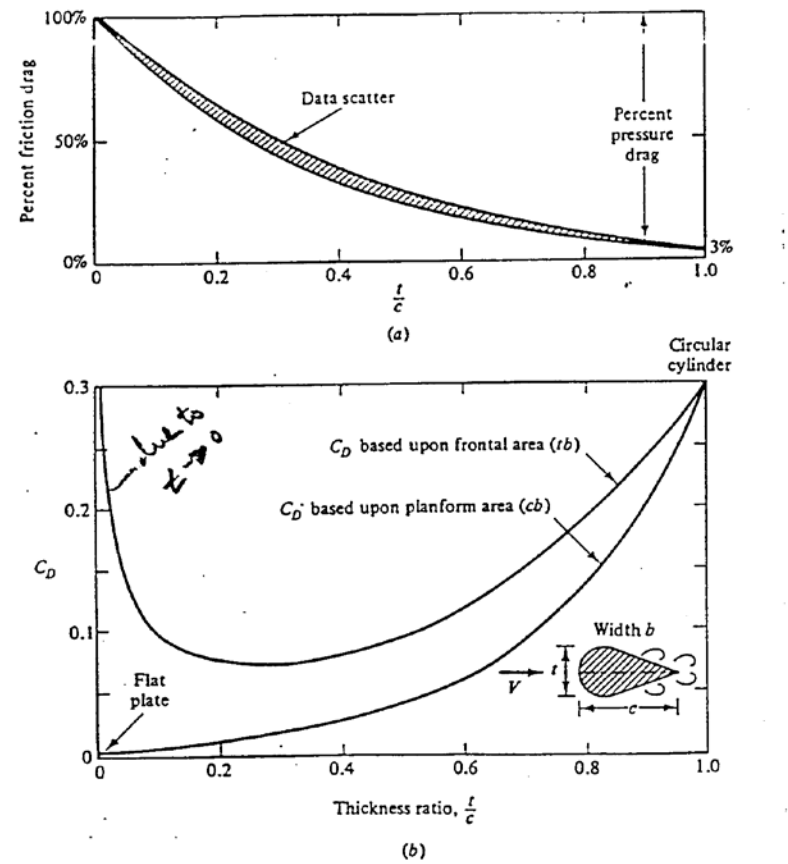

Fig. 7.12 Drag of a streamlined two-dimensional cylinder at $Re_c = 10^6$: (a) effect of thickness ratio on percentage friction drag; (b) total drag versus thickness when based upon two different areas.

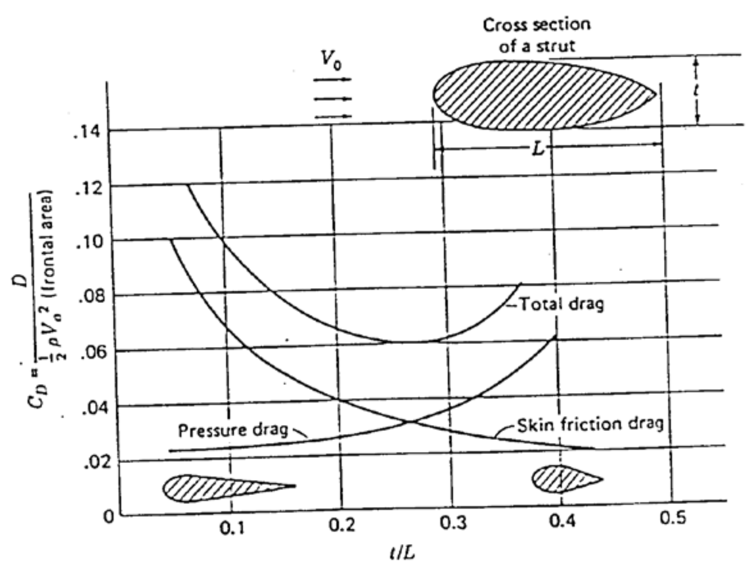

Figure 10.24 Drag coefficients for a family of struts. (*S. Goldstein, "Modern Developments in Fluid Dynamics," Dover Publications, New York, 1965.*)

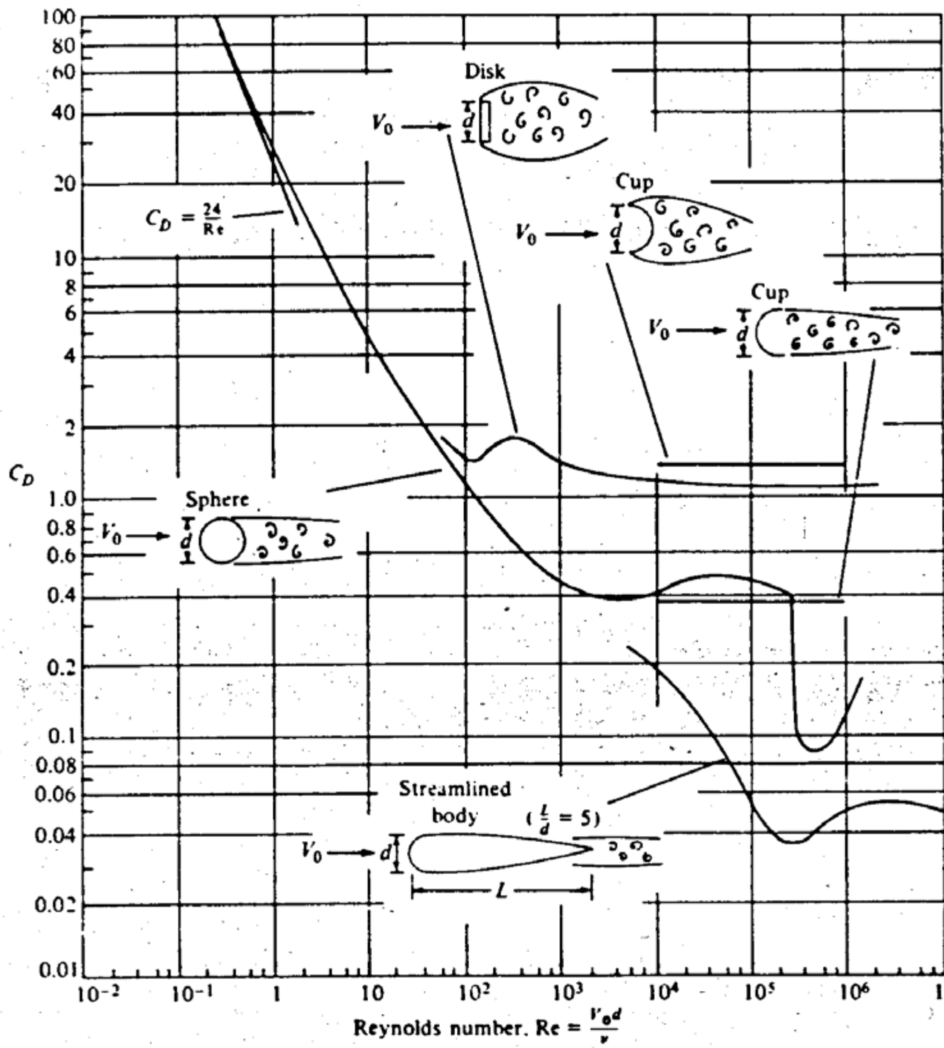

FIGURE 11-11 Coefficient of drag versus Reynolds number for axisymmetric bodies. [Data sources: Abbott (1), Breevoort (4), Freeman (9), and Rouse (24).]

Table 7.3

DRAG OF THREE-DIMENSIONAL BODIES AT Re ≈ 10^5

Body	*Ratio*	C_D *based on frontal area*	
Cube:			
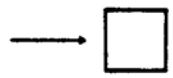		1.07	
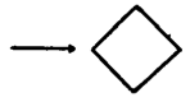		0.81	
60° cone:			
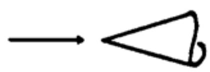		0.5	
Disk:			
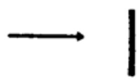		1.17	
Cup:			
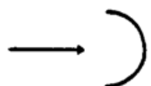		1.4	
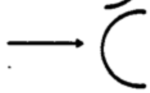		0.4	
Parachute (low porosity):			
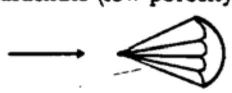		1.2	
Rectangular plate:			
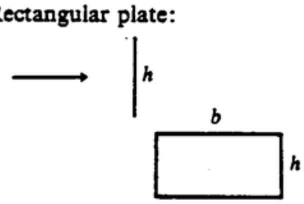	b/h 1	1.18	
	5	1.2	
	10	1.3	
	20	1.5	
	∞	2.0	
Flat-faced cylinder:			
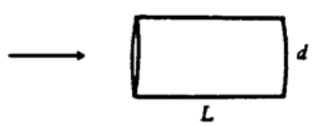	L/d 0.5	1.15	
	1	0.90	
	2	0.85	
	4	0.87	
	8	0.99	
Ellipsoid:		*Laminar*	*Turbulent*
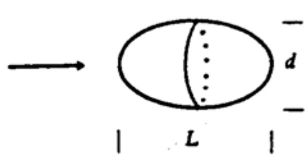	L/d 0.75	0.5	0.2
	1	0.47	0.2
	2	0.27	0.13
	4	0.25	0.1
	8	0.2	0.08

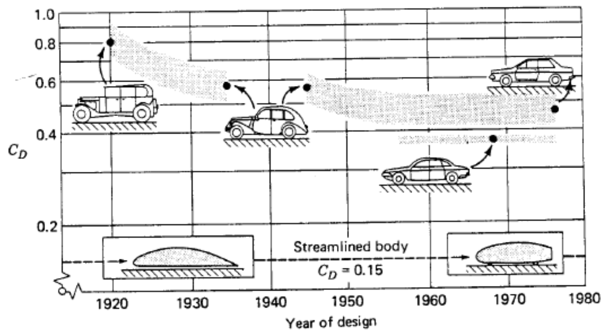

Figure 10.25 Time history of the aerodynamic drag of cars in comparison with streamlined bodies. (*From Hucho, W. H., Janssen, L. J., Emmelmann, H. J., 1976, "The Optimisation of Body Details—A Method For Reducing The Aerodynamic Drag of Road Vehicles," SAE 760185.*)

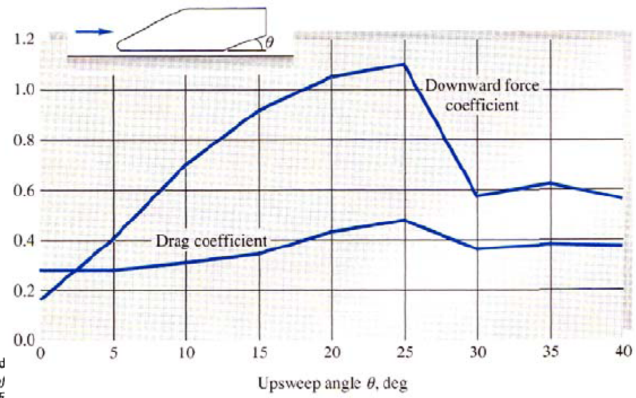

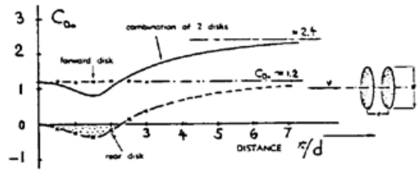

Figure 1. Interaction between two disks placed one behind the other; (reference 1,a).

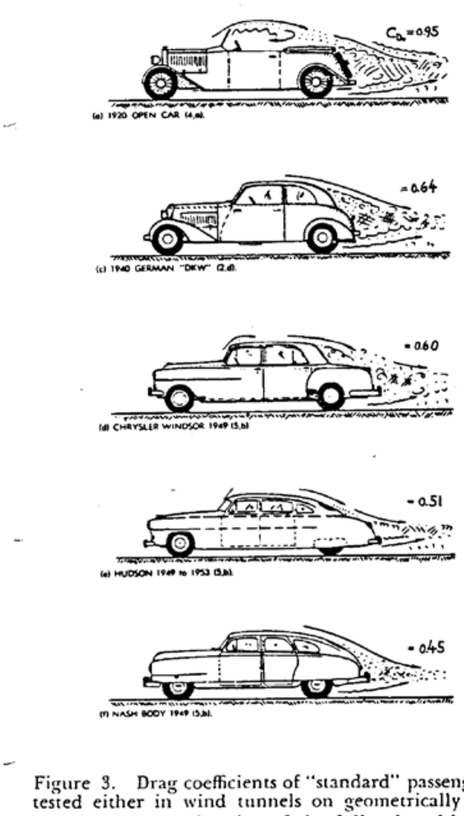

Figure 3. Drag coefficients of "standard" passenger cars, tested either in wind tunnels on geometrically similar models or by deceleration of the full-scale vehicles.

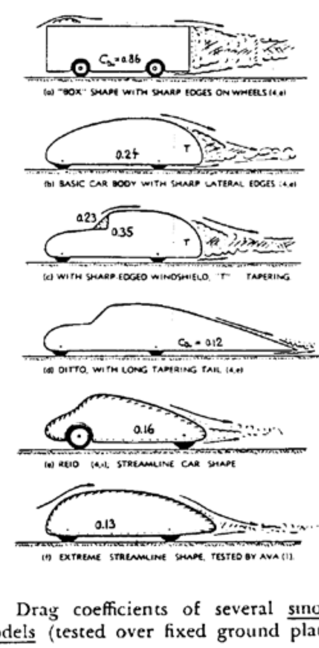

Figure 4. Drag coefficients of several smooth wind tunnel models (tested over fixed ground plate).

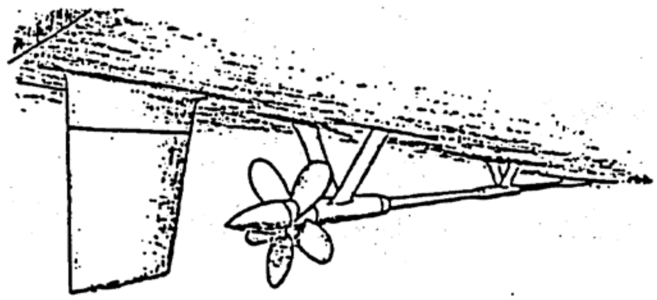

Figure 2-4. Typical naval ship stern appendages (from Kirkman, et al., 1979)

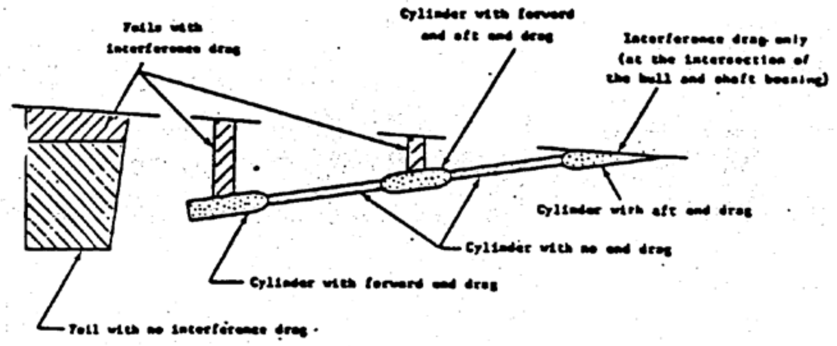

Figure 2-5. Appendage decomposition (from Kirkman, et al., 1979)

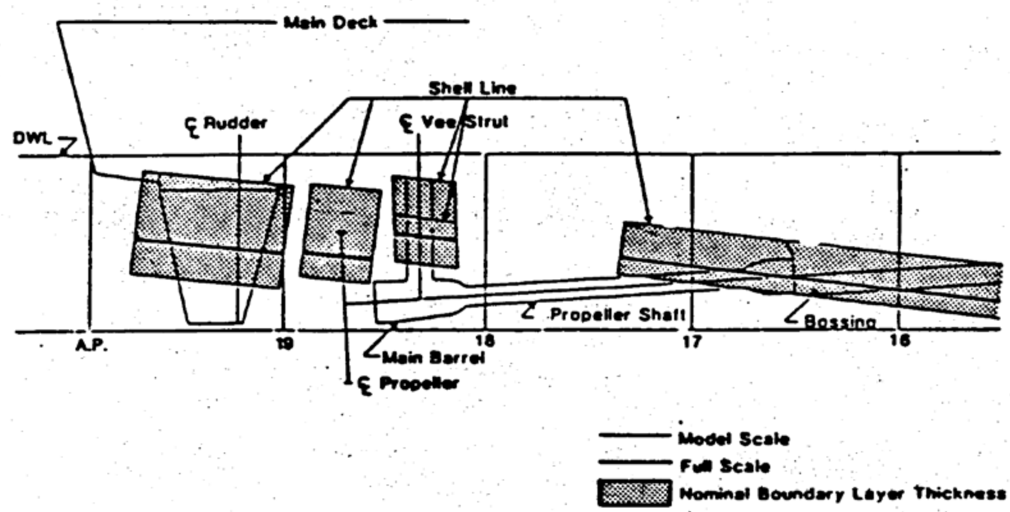

Figure 2-6. Nominal boundary layer thickness in way of the DDG 51 appendages.

Terminal Velocity

Terminal velocity is the maximum velocity attained by a falling body when the drag reaches a magnitude such that the sum of all external forces on the body is zero. Consider a sphere using Newton' Second law:

$$\sum \underline{F} = F_d + F_b - F_g = m\underline{a}$$

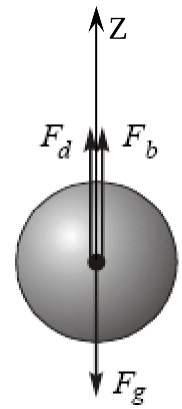

when terminal velocity is attained

$\sum \underline{F} = \underline{a} = 0$:

$$F_d + F_b = F_g$$

or

$$\frac{1}{2}\rho V_0^2 C_D A_p = \left(\gamma_{Sphere} - \gamma_{fluid}\right)\cancel{V}_{Sphere}$$

For the sphere

$$A_p = \frac{\pi}{4}d^2 \text{ and } \cancel{V}_{Sphere} = \frac{\pi}{6}d^3$$

The terminal velocity is:

$$V_0 = \left[\frac{\left(\gamma_{sphere} - \gamma_{fluid}\right)\left(4/3\right)d}{C_D \rho_{fluid}}\right]^{1/2}$$

<u>Magnus effect:</u> Lift generation by spinning

Breaking the symmetry causes the lift!

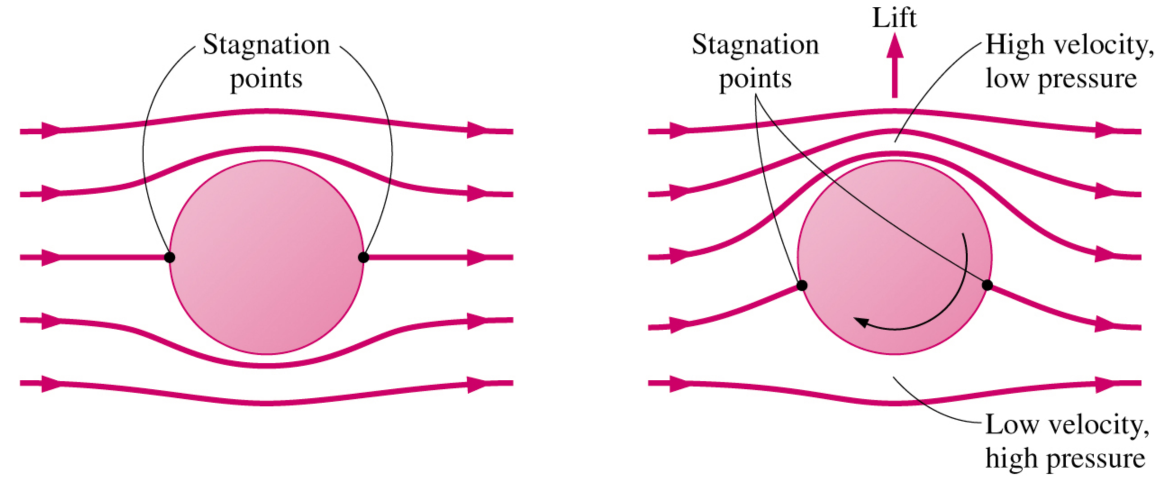

(*a*) Potential flow over a stationary cylinder (*b*) Potential flow over a rotating cylinder

Effect of the rate of rotation on the lift and drag coefficients of a smooth sphere:

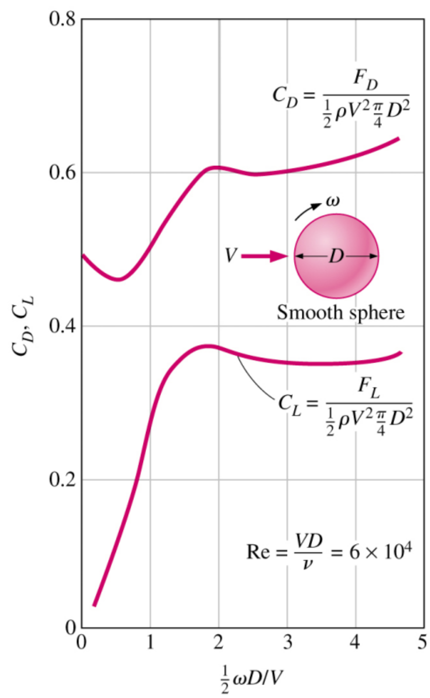

Lift acting on the airfoil

Lift force: the component of the net force (viscous+pressure) that is perpendicular to the flow direction

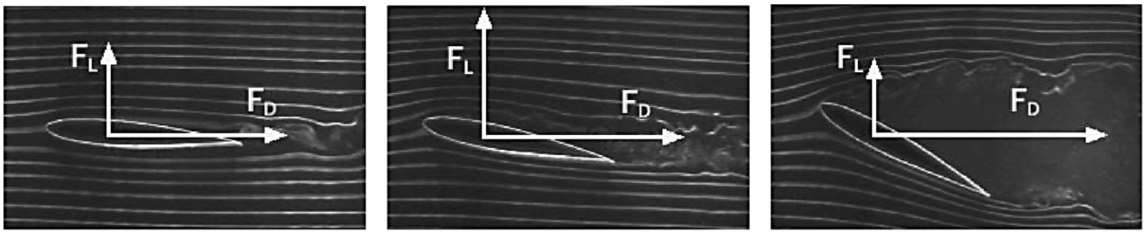

(a) 5° (b) 15° (c) 30°

Variation of the lift-to-drag ratio with angle of attack:

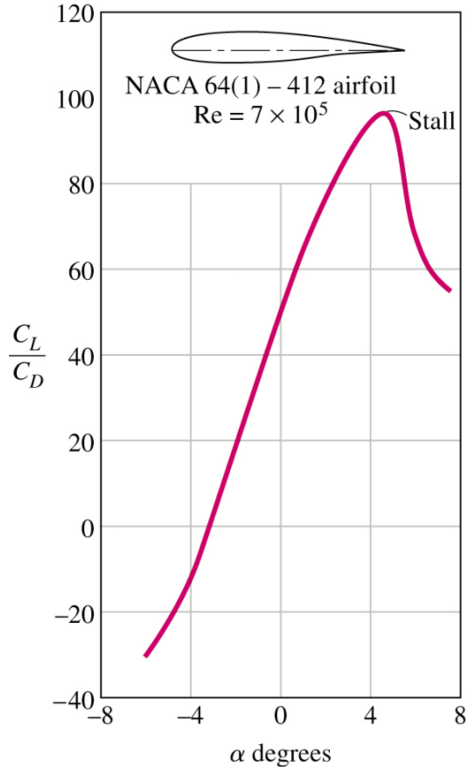

The minimum flight velocity:

→Total weight W of the aircraft be equal to the lift

$$W = F_L = \frac{1}{2} C_{L,\max} \rho V_{\min}^2 A \rightarrow V_{\min} = \sqrt{\frac{2W}{\rho C_{L,\max} A}}$$

Effect of Compressibility on Drag: CD = CD(Re, Ma)

$$Ma = \frac{U_\infty}{a}$$

speed of sound = rate at which infinitesimal disturbances are propagated from their source into undisturbed medium

Ma < 1	subsonic	≤ 0.3 flow is incompressible, i.e., ρ ~ constant
Ma ~ 1	transonic (=1 sonic flow)	
Ma > 1	supersonic	
Ma >> 1	hypersonic	

C_D increases for Ma ~ 1 due to shock waves and wave drag

$Ma_{critical}$(sphere) ~ .6

$Ma_{critical}$(slender bodies) ~ 1

For U ≥ a: upstream flow is not warned of approaching disturbance which results in the formation of shock waves across which flow properties and streamlines change discontinuously

FIGURE 11.12
Drag characteristics of projectile, sphere, and cylinder with compressibility effects. [After Rouse (26)]

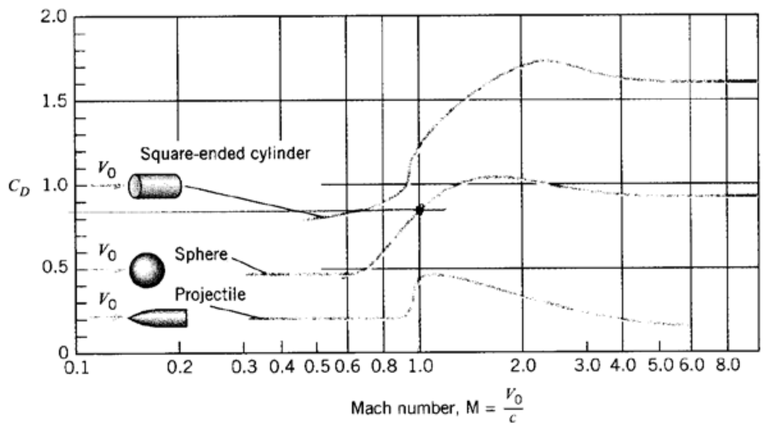

FIGURE 11.13
Contour plot of the drag coefficient of the sphere versus Reynolds and Mach numbers.